Probing Semiconductor Gap States with Resonant Tunneling

S. Loth,[1] M. Wenderoth,[1,*] L. Winking,[1] R. G. Ulbrich,[1] S. Malzer,[2] and G. H. Döhler[2]

[1]*IV. Physikalisches Institut der Universität Göttingen, Friedrich-Hund-Platz. 1, 37077 Göttingen, Germany*

[2]*Max-Planck-Research Group, Institute of Optics, Information, and Photonics, Universität Erlangen-Nürnberg, 91058 Erlangen, Germany*

(Received 8 June 2005; published 15 February 2006)

Tunneling transport through the depletion layer under a GaAs {110} surface is studied with a low temperature scanning tunneling microscope (STM). The observed negative differential conductivity is due to a resonant enhancement of the tunneling probability through the depletion layer mediated by individual shallow acceptors. The STM experiment probes, for appropriate bias voltages, evanescent states in the GaAs band gap. Energetically and spatially resolved spectra show that the pronounced anisotropic contrast pattern of shallow acceptors occurs exclusively for this specific transport channel. Our findings suggest that the complex band structure causes the observed anisotropies connected with the zinc blende symmetry.

DOI: 10.1103/PhysRevLett.96.066403 PACS numbers: 71.55.Eq, 73.20.−r, 73.40.Gk

The basic properties of the electronic band structure of semiconductors with zinc blende symmetry like GaAs can be described by only including the cubic symmetry. Effects going beyond this due to the lack of the inversion symmetry are known, but are usually considered to be small, e.g., k-linear terms [1]. A long-standing puzzle in this context is the strong anisotropic contrast of shallow acceptors in III-V semiconductors as they are imaged by scanning tunneling microscopy (STM): while donors exhibit circular symmetric contrasts [2] and the deep acceptor Manganese shows a crosslike shape compatible with the cubic symmetry [3], shallow acceptors like carbon (see Fig. 1), zinc, beryllium, and cadmium [4–6] appear as distinct triangular protrusions. With the dopant site located in the triangle's tip the breaking of cubic symmetry is even more pronounced. A recent Letter states that this mystery can be attributed to the wave function mapping of an excited acceptor state [6]. This implies a model solely based on the real part of the band structure. In contrast to this interpretation our data indicate that not the real part but the complex part of the band structure resembles in a prominent way the zinc blende symmetry of the underlying crystal, leading to the large deviation from the cubic symmetry. The presented measurements show that the triangular contrasts are due to a resonant tunneling process involving evanescent sample states and that at no sample bias voltage an elongated contrast which is compatible with the cubic symmetry is observed.

For the experiment a heterostructure consisting of a homogeneously carbon doped GaAs layer grown by molecular beam epitaxy (MBE) on a (001)-oriented zinc doped GaAs substrate was chosen. The doping concentrations for both elements were $5 \times 10^{18}/\mathrm{cm}^3$. The Zn and C doped regions were separated by an AlGaAs marker layer. Because of this sample design the investigation of C and Zn acceptors with the same tip configuration on the same sample was possible. The samples were *in situ* cleaved along a {110} plane at a base pressure better than 2×10^{-11} mbar and cooled down to 8 K immediately afterwards [7]. In large scale scans surrounding the region of interest every defect is characterized. The spatially resolved $I(V)$ spectroscopy measurements (STS) are performed at least 15 nm away from defects any other than acceptors. The tip sample distance is fixed at a carefully chosen tunneling set point where the acceptors have nearly no impact on the topography, thus avoiding topographic artefacts. All $I(V)$ spectra shown here are normalized to a plane of constant tip height, using the simultaneously recorded work function and topography [8]. The projected positions of the dopant atoms beneath the surface are indicated by a white circle in the respective images. They are determined by the center of mass of the circular contrasts at high positive or negative sample voltages to an accuracy better than one surface unit cell [4].

In Fig. 2 the results of an STS measurement performed on a carbon doped region are shown. One of the $I(V)$ characteristics is taken above the region of the triangular contrast, the other several nanometers away on a region

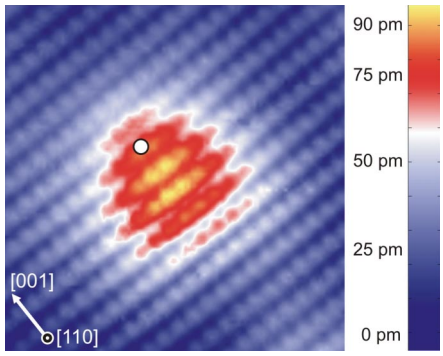

FIG. 1 (color online). $(7.1 \times 7.1)\ \mathrm{nm}^2$ STM image of a single carbon acceptor near the (110) surface of GaAs. The image was acquired simultaneously with a STS measurement at sample voltage +1.5 V and current set point 600 pA. The white circle indicates the position of the dopant atom beneath the surface

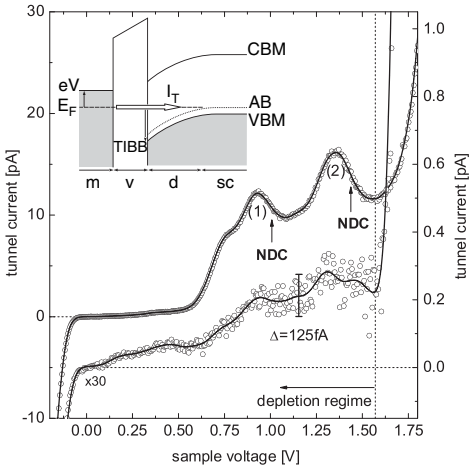

FIG. 2. $I(V)$ characteristics of a buried carbon acceptor (upper curve) and the undisturbed surface (lower curve) obtained by spatially resolved $I(V)$ spectroscopy (STS). The raw data are plotted as points, averaged data as lines. The $I(V)$ curve taken on the undisturbed surface is scaled by a factor of 30 with respect to the one taken on the C acceptor. Note that the spectroscopic features indexed with (1) and (2) are followed by negative differential conductivity (NDC). Noise level for both curves is smaller than 125 fA. The inset sketches the energetic conditions of the depletion layer regime in the voltage interval from 0 V to 1.57 V in a rigid-band model: (m) metallic tip, (v) vacuum barrier, (d) depletion layer, (sc) bulk semiconductor, ($TIBB$) depletion barrier height, (VBM) valence band maximum, (CBM) conduction band minimum, (AB) acceptor band, and (I_T) tunneling channel.

where no acceptor related contrast is visible. Both $I(V)$ curves yield semiconductor characteristics with valence (negative voltage) and conduction (voltage larger than $+1.5$ V) band components separated by a band gap region of about 1.5 V. Above the topographic carbon contrast (Fig. 1) two groups of peaks are visible with a spectral weight of more than 10% of the set point current (150 pA) and an onset of the tunnel current as low as 0.3 V. The first group denoted with (1) in Fig. 2 relates to peaks in the differential conductivity dI/dV lying at 682 mV and 870 mV, and the second group marked with (2) relates to a peak at 1250 mV. The $I(V)$ curve recorded on the undisturbed surface is magnified by a factor of 30 with respect to the one recorded above the acceptor, and reveals the same characteristic shape lying well above the noise level of the raw data points of about 125 fA. Similar measurements on zinc acceptors as shown in Fig. 3 exhibit the same behavior. Two facts should be pointed out: considering the potential configuration in the band gap regime, i.e., depletion (see inset of Fig. 2), it is surprising to observe such high conductivity. But most striking is the observation of negative differential conductivity (NDC) causing a negative slope of the $I(V)$ curve in the voltage intervals from 932 mV to 1080 mV and from 1357 mV to 1559 mV. It is important to note that the observation of NDC cannot be

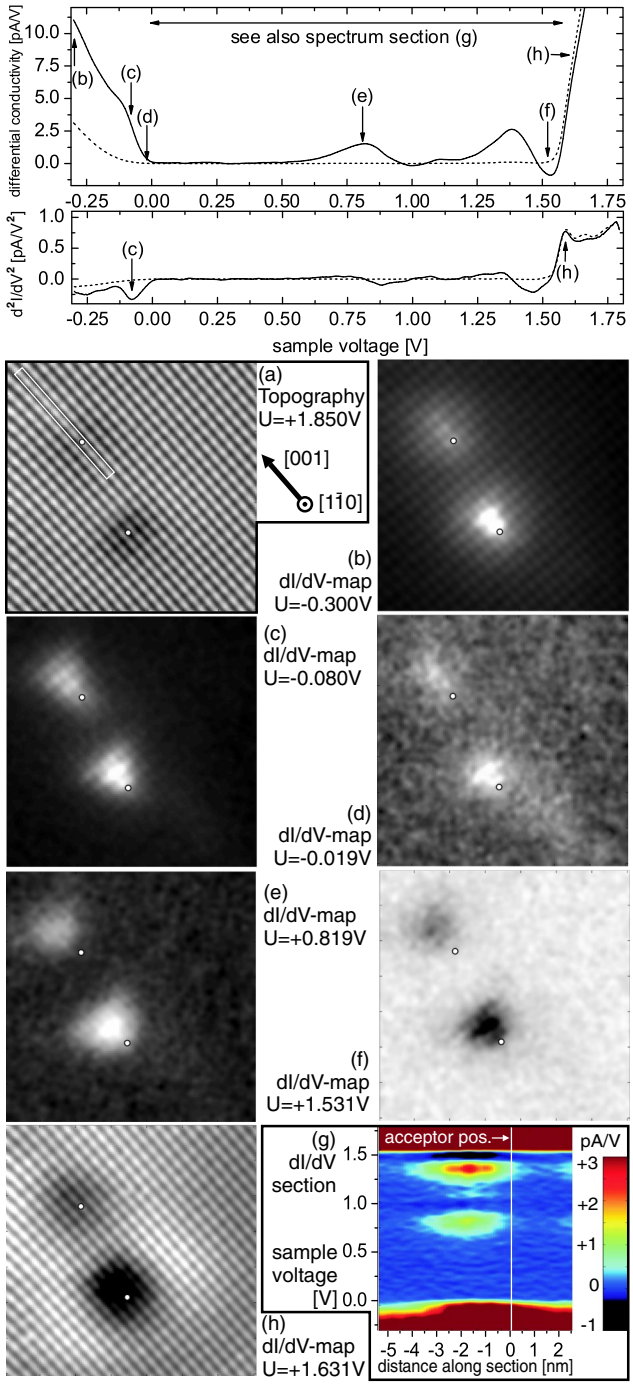

FIG. 3 (color online). Spatially resolved $I(V)$ spectroscopy of two buried zinc acceptors near the $(1\bar{1}0)$ surface: (a) simultaneously recorded topographic image at set point voltage $+1.85$ V and current 1 nA. (above) Differential conductivity spectra and excitation spectra dI^2/dV^2 are acquired above one of the triangular contrasts (solid line) and above the undisturbed surface (dashed line) in the upper right corner of the imaged area. dI/dV maps: (b)–(e) Regions of enhanced conductivity shown in white, (f) NDC shown in black, (h) charge density oscillations around the acceptor atoms. dI/dV section (g) showing energy dependent change in contrast extension. The cross section is indicated by a white rectangle in (a). Projected dopant atom positions are marked by white circles.

described with the commonly employed tunneling theory. Therefore, the measured current is not only determined by the sample LDOS, a more detailed description of the transport mechanism is needed.

To identify the origin of the acceptor induced conductivity the potential configuration along the tunnel path has to be evaluated. By solving the Poisson's equation as explained in Ref. [9] this question can be addressed. Parameters are: 4.0 eV work function, which was experimentally obtained by dI/dz measurements at the tunneling set point, tip sample distance 7 Å, low temperature GaAs band gap 1.52 eV, and electron affinity 4.1 eV [10], p-doping concentration $5 \times 10^{18}/\mathrm{cm}^3$, and 26 meV or 31 meV ionization energy for C or Zn, respectively [11]. We find an almost linear dependence of the surface potential of the semiconductor space charge region with the applied sample voltage [so-called tip induced band bending, $TIBB(V)$ [12]] having flat band condition, i.e., $TIBB = 0$ V, at sample voltage $+1.57$ V. For voltages lower than $+1.57$ V the semiconductor surface is in depletion, i.e., downwards bending of the bands (negative $TIBB$). At higher voltages the surface layer is in accumulation (positive $TIBB$). This calculated behavior agrees with the STS measurements. In the "excitation spectra" d^2I/dV^2 taken above the undisturbed surface and a zinc acceptor, respectively, which are plotted in Fig. 3, we find a prominent peak denoted with (h) at 1586 mV in both spectra. In addition to that, we find valence band related corrugation for slightly lower voltage [see Fig. 3(f) sample voltage 1531 mV] and conduction band related corrugation together with charge density oscillations [see also [2,7,13]] centered around the dopant atom's position for slightly higher voltage [see Fig. 3(h) sample voltage 1631 mV].

Starting from the empirical knowledge of the potential configuration we can now focus on the development of a model for "band gap conductivity" from 0 V to 1.5 V. The two groups of peaks denoted with (1) and (2) in Fig. 2 and with (e) and (f) in Fig. 3 belong to electrons tunneling from the tip through the vacuum gap and the depletion layer into the bulk of the crystal. The doping concentration of $5 \times 10^{18}/\mathrm{cm}^3$ causes an impurity band of $\sim$10 meV spectral width [11] centered $\sim$30 meV above the valence band edge. As depicted in the inset of Fig. 2 injected carriers are drained through the acceptor band (AB) and the samples are conducting even at 4.2 K. At low temperatures the band is partially filled and the tunnel path is energetically pinned within it (I_T). In this regime, neither valence band nor conduction band real states participate in the tunneling process at the surface. The tunnel current becomes dependent only on the transmission probability through this structure. In the vicinity of an acceptor the potential landscape U is modified by the dopant's unscreened charge in a way sketched in the inset of Fig. 4. To estimate the quantum mechanical transmission

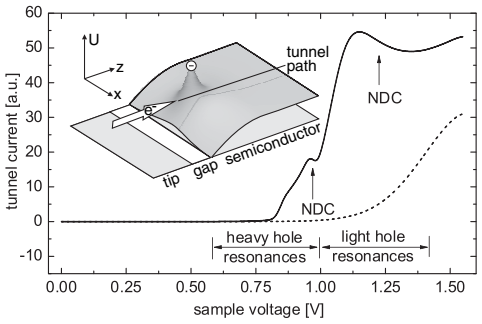

FIG. 4. Numerical simulation of the tunnel current for an acceptor buried five monolayers beneath the surface (solid line) and the undisturbed surface (dashed line). The light hole and heavy hole contribution to the transmission is indicated, as are the two intervals of negative differential conductivity (NDC). The inset depicts the potential situation along the tunneling path in the vicinity of an acceptor according to the inset in Fig. 2.

through this system, we employ the 1-d transfer matrix technique and model the potential along a straight tunnel path perpendicular to the surface with stepwise constant potentials [14]. To describe the transport through the metal vacuum semiconductor interface, the effective mass approximation is used and the Ben Daniel Duke boundary conditions are applied to the interfaces [15].

The tunnel current is calculated as a function of the height of the depletion layer potential ($TIBB$) and rescaled to the sample voltage using the $TIBB(V)$ relation (Fig. 4). For a quantitative evaluation of the tunnel current's spatial distribution, a full 3-d calculation would be needed, which is not developed at present. But the employed model already gives qualitative trends: for large distances, i.e., in the absence of an acceptor, the $I(V)$ curve is monotonous and shows negligible current up to 1 V. But in the vicinity of the acceptor, i.e., averaged over distances smaller than 1 nm, the tunnel current shows two regions of enhanced conductivity, one lying below 1.0 V and one above 1.0 V sample voltage. Such transmission enhancements are attributed to a buildup of resonances in the acceptor potential. It is worth noting that the NDC observed in the measurements is a good indicator for a resonant process. No other theory involving tunneling on semiconductors known to us [e.g., a special interplay of $TIBB$ with heightening of the vacuum barrier, sequential tunneling through acceptor states, or rate equations [16]] can create such an $I(V)$ characteristic.

The $I(V)$ characteristics taken above carbon acceptors (Fig. 2) and zinc acceptors (Fig. 3) look alike. Comparing the simulation (Fig. 4) with the measurements we find good qualitative agreement for positions close to the acceptor. Both curves show two regions of enhanced tunnel current followed by negative differential conductivity. The simulation includes the light hole and heavy hole valence bands by constant effective masses. Although this procedure is very approximate, it points to an interesting effect: within

the crude approximation the peaks (1) and (2) in Fig. 2 can be identified as heavy hole and light hole resonances, respectively, separated up to 560 meV from each other, suggesting the capability to map energetic properties of the participating sample states with the STM. For a homogenously doped sample with a doping density of $5 \times 10^{18}/\mathrm{cm}^3$, an average extension of the triangular contrast of about 10 nm for the deepest buried acceptor that can be detected with the STM (8th monolayer under the surface) and an average thickness of the depletion layer between 5–10 nm there is no point on the surface on which a tunnel path perpendicular to the surface is not influenced by at least one acceptor. Therefore, we also attribute the conductivity measured above the undisturbed surface to acceptors buried below the detection limit of topographic STM techniques but well within the resolution of STS measurements.

The tunnel current is mediated by bulk sample states energetically located within the band gap, i.e., by evanescent states described within the framework of the complex band structure. The acceptor's Coulomb potential in the depletion layer forms resonant tunneling paths that allow for the detection of the otherwise vanishing gap state conductivity. Laterally resolved STS measurements reveal the extension of the resonant tunnel paths. Conductivity maps from -0.3 to $+1.57$ V sample bias [Fig. 3 maps (b) to (f)] point out that the enhanced conductivity and the NDC are restricted to a triangular region shifted laterally away from the position of the dopant atom. According to the calculated $TIBB(V)$ dependence [based on [9,12]] the sample is in depletion for these voltages. This gives evidence that the interval of resonant transport coincides with the observation of triangular contrasts [17]. At flat band voltage real sample states become available at the surface. A change in contrast symmetry to circular symmetric features centered above the dopant atom's position occurs together with the change in tunneling conditions [see transition from map (f) to (h)]. Similarly, when the sample reaches the inversion limit for large negative voltages a circular protrusion is imaged [4]. The circular features resemble the electrostatic influence of the stationary charge on the valence and conduction band.

Recently [6] suggested that the triangular shaped contrasts recorded with the STM represent a kind of cross section through the three-dimensional squared wave functions of excited acceptor states. The vacuum barrier height is a crucial parameter for this interpretation, because it directly influences the connection between sample bias voltage and its energetic levels ($TIBB$). We experimentally determined this value for each tip configuration, and confirmed the derived $TIBB(V)$ behavior with respect to voltage dependent corrugation changes, onset of charge density oscillations, and other spectroscopic features [17]. Our measurements cover the same energy interval like [6] and give strong indication that the contrasts are mainly caused by the bulk related conduction mechanism through evanescent states, rather than by the direct imaging of an excited acceptor state. It remains to be evaluated, whether donors and deep defects in III-V semiconductors like Si [2] and Mn [3] are imaged similarly.

The energy resolved cross section (g) in Fig. 3 shows that the lateral extension of the probed evanescent states changes with varying sample voltage, suggesting that structural anisotropies of the complex band structure become apparent. Further measurements on acceptors in different subsurface layers show that the conductance maximum shifts along $\langle 112 \rangle$ directions throughout the crystal.

We conclude that due to the process of resonant tunneling (for appropriate tunneling set points) the local STM probe visualizes anisotropic properties of evanescent sample states. The presented measurements indicate that energy dependent features can be resolved by tuning the space charge region at the surface. The involvement of evanescent sample states gives rise to highly anisotropic features resembling in a prominent way the zinc blende symmetry of the underlying crystal, which points to the importance of the complex band structure for tunneling processes in semiconductors.

The authors thank P. M. Koenraad and M. E. Flatté for valuable discussions. This work was supported by the DFG, SFB 602, and the German National Academic Foundation.

*Electronic address: wendero@ph4.physik.uni-goettingen.de

[1] M. Cardona, N. E. Christensen, and G. Fasol, Phys. Rev. Lett. **56**, 2831 (1986).
[2] R. M. Feenstra *et al.*, Phys. Rev. B **66**, 165204 (2002).
[3] A. M. Yakunin *et al.*, Phys. Rev. Lett. **92**, 216806 (2004).
[4] R. de Kort *et al.*, Phys. Rev. B **63**, 125336 (2001).
[5] J. F. Zheng, M. Salmeron, and E. R. Weber, Appl. Phys. Lett. **64**, 1836 (1994).
[6] G. Mahieu *et al.*, Phys. Rev. Lett. **94**, 026407 (2005).
[7] M. Wenderoth *et al.*, Europhys. Lett. **45**, 579 (1999).
[8] J. K. Garleff *et al.*, Phys. Rev. B **70**, 245424 (2004).
[9] G. J. de Raad *et al.*, Phys. Rev. B **66**, 195306 (2002).
[10] S. Adachi, *GaAs and Related Materials Bulk Semiconducting and Superlattice Properties* (World Scientific, Singapore, 1994).
[11] E. F. Schubert, *Doping in III-V Semiconductors* (Cambridge University Press, Cambridge, England, 1993).
[12] R. M. Feenstra and J. A. Stroscio, J. Vac. Sci. Technol. B **5**, 923 (1987).
[13] R. Dombrowski *et al.*, Phys. Rev. B **59**, 8043 (1999).
[14] P. Harrison, *Quantum Wells, Wires and Dots* (Wiley, New York, 2000).
[15] G. T. Einevoll and L. J. Sham, Phys. Rev. B **49**, 10 533 (1994).
[16] X. de la Broïse *et al.*, Phys. Rev. B **61**, 2138 (2000).
[17] A full treatment of the comprehensive spectroscopic data will be given elsewhere.